NUMERICAL SIMULATION OF HEAT TRANSFER AND PRESSURE DROP CHARACTERISTICS IN TWISTED OVAL TUBES

Xichao DI[a], Ping TAO[a], Meihui ZHOU[a], Jianqiu ZHOU[a*]

[a] School of Energy Science and Engineering, Nanjing Tech University, Nanjing, Jiangsu Province, 210000, China.

[*] Corresponding author; E-mail: zhouj@njtech.edu.cn

The numerical research aims to investigate the heat transfer performance difference between the twisted tube and the smooth tube at the same hydraulic diameter. The effect of the major/minor axis ratios on the fluid flow inside the twisted oval tube is studied in the Reynolds number range of 3000-11000, and the integral thermal-hydraulic effectiveness of twisted oval tubes is evaluated. The results show that the twisted wall induces secondary flow perpendicular to the mainstream direction. The vortices are rapidly generated in the pipeline when the fluid enters the twisted tube section from the upstream section. As the fluid develops further, the vortices converge to form a spiral flow. Numerical simulations indicate that the average Nusselt number of twisted oval tube with a major/minor axes ratio of 1.70 increases by 18.7%-35.5%, while the pressure drop increases by 59.9%-61.3% compared to smooth oval tube. Furthermore, as the major/minor axes ratio increases from 1.18 to 2.48, the average Nusselt number experiences an increase of 26.7%-38.2%. The twisted tubes within the major/minor axes ratio range of 1.40 to 1.96 demonstrate superior integral thermal-hydraulic performance compared to other pipes.

Key words: *Twisted oval tube; Heat transfer; Pressure drop; Integral thermal-hydraulic effectiveness*

1. Introduction

As key equipment for energy utilization and transmission, heat exchangers are widely utilized in diverse industries, including petrochemicals, power generation, equipment manufacturing and air conditioning [1-4]. However, the dissipative effect of energy transfer leads to irreversible energy loss [5]. Therefore, developing efficient heat transfer equipment becomes a hot topic in the field of energy utilization. A twisted oval tube (TOT) is a passive enhancement heat transfer element. It is a heat transfer tube structure with an elliptical cross-section obtained by compressing and twisting a circular tube. As early as the 1980s, TOT heat exchangers were developed to improve the energy utilization efficiency of thermal cycle systems [6, 7]. As a highly efficient heat transfer device, TOTs offer the benefits of efficient thermal conductivity and comparatively small flow resistance. According to usage data provided by the petrochemical industry, TOT heat exchangers have the potential to achieve production costs savings of roughly 25% compared to traditional baffle plate heat exchangers [8].

In recent years, many scholars have researched the enhanced heat transfer mechanism of TOT by experiments and numerical simulations. The study revealed the fluid inside the TOT flows in a

helical pattern, resulting in transverse flow components perpendicular to the primary flow direction [9]. This increases the turbulence intensity, thereby increasing the heat transfer efficiency between the fluid and the heat tube wall. Yang et al. [10] studied the heat transfer and resistance characteristics of water flow in TOTs with different structural dimensions using experimental methods, and proposed a unified correlation formula to predict the heat transfer coefficient and friction coefficient. The experimental results showed that larger major/minor axis ratios (a/b) and smaller twist spacings would significantly enhance the heat transfer and flow resistance. Tan et al. [11] analyzed the enhanced heat transfer mechanism of TOT using the field synergy principle. The results demonstrated that the generation of secondary flow reduced the synergistic angle between the velocity vector and temperature gradient, thereby improving the heat transfer performance of TOT. Cheng et al. [12] used numerical simulation methods to study the flow characteristics of water in the TOT with Re ranging from 50 to 2000, and determined that the transition point from laminar to turbulent flow occurs at a Re of 500. Guo et al. [13, 14] researched the laminar heat transfer inside TOT under uniform wall temperature boundary conditions and uniform heat flux boundary conditions using numerical simulation methods, and established a correlation between the secondary flow intensity and the flow friction coefficient and average Nusselt number ($\overline{Nu}$). They also found that local *Nu* had distinctive properties in different measured areas of TOT. Wu et al. [15] simulated the effects of different twist spacings and Re on the pressure drop and heat transfer characteristics of TOT. The results showed that TOT with twist spacing of 128 mm had better integral thermal-hydraulic effectiveness than those with twist spacing of 96 mm and 192 mm.

Several researchers have also investigated the flow characteristics of fluid outside the TOT. Gu et al. [16, 17] investigated the TOT heat exchanger with the novel coupling-vortex chessboard tube layout using numerical simulations, and innovatively designed an alternate V-rows triangular tube design. Li et al. [18, 19] experimentally analyzed the shell side performances of staggered TOT heat exchanger and derived the relationships between Nusselt number and Euler number. They also compared the shell-side thermal performance of heat exchangers consisting of TOTs only and TOTs combined with round tubes by numerical simulations. Gu et al. [20] used the field synergy principle to analyze the shell-side performance of TOT heat exchanger with a helical baffle. Luo et al. [21] concluded numerical simulations to study the flow characteristics inside a double twisted ring with opposite twist directions, and studied the heat transfer performance under different geometric dimensions.

In contrast to the traditional circular tube bundle heat exchanger, the TOT heat exchanger exhibits significantly improved heat transfer performance. Therefore, it is necessary to investigate the impact of the twisted structure on the enhancement of heat transfer performance. In this study, we ensure that the hydraulic diameter of different tubes is equal. This decision is based on the following considerations: when comparing the heat transfer and pressure drop performance of different tubes under fixed Re, inconsistent hydraulic diameters result in different fluid velocities inside the tubes. Higher fluid velocities lead to increased temperature differences between the fluid and the tube wall, thereby improving the heat transfer rate and overall heat transfer coefficient of the tubes. Therefore, to avoid the influence of this factor, all tubes are standardized with the same hydraulic diameter [22]. Through this approach, we better understand the impact of geometric differences on tube performance. In addition, this study also summarizes the formation process of spiral flow, further revealing the enhanced heat transfer mechanism of TOT.

2. Model description

2.1. Physical model

This work establishes the smooth circular tube (SCT), smooth oval tube (SOT) and TOT models. The primary geometric elements of TOT are the major axis (a) and minor axis (b) of the tube cross-section, the twist spacing (S), and the tube length (L). The a/b of the TOTs investigated in the research scope from 1.18 to 2.48, and the twist spacing is 128mm. The length of all tubes is 640mm, and the hydraulic diameter is 19.7mm. The inlet extension section (L_{in}) and outlet extension section (L_{out}) are added at the inlet and outlet of the pipeline model to ensure that the flow state of the fluid as it enters the pipeline is completely developed and that there is no backflow at the outlet cross-section of the pipeline. The tube models of the extension section are smooth tubes with a length of 5 times the hydraulic diameter of the tube. The physical model of the TOT is shown in Figure 1.

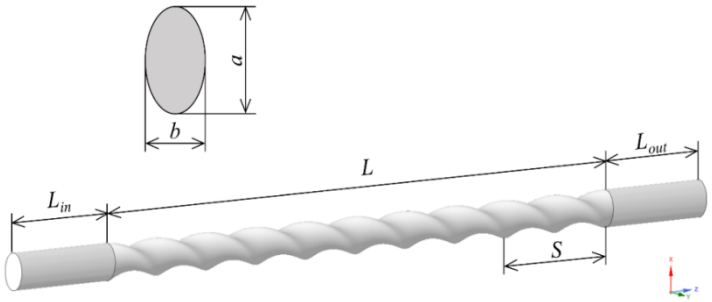

Figure 1. Physical model of the TOT.

2.2. Mathematic model

The working fluid is uncompressible. The control equations for completely developed turbulent fluid are as follows:

$$\frac{\partial \rho}{\partial t}+\frac{\partial(\rho u_j)}{\partial x_j}=0 \tag{1}$$

$$\rho\frac{\partial u_i}{\partial t}+\rho u_j\frac{\partial u_i}{\partial x_i}=-\frac{\partial p}{\partial x_i}+\mu\frac{\partial}{\partial x_j}\left(\frac{\partial u_i}{\partial x_j}+\frac{\partial u_j}{\partial x_i}\right) \tag{2}$$

$$\rho\frac{\partial T}{\partial t}+\rho\frac{\partial(u_i T)}{\partial x_i}=-p\frac{\partial u_i}{\partial x_i}+\lambda\frac{\partial}{\partial x_j}\left(\frac{\partial u_i}{\partial x_j}+\frac{\partial u_j}{\partial x_i}\right) \tag{3}$$

where ρ, μ and λ are the density, dynamic viscosity, and thermal conductivity, respectively.

The standard k-ω model is selected for modeling turbulent flow in the pipeline. The rationale for this choice will be explained later. The control equations for k and ω are expressed below:

$$\rho\frac{\partial k}{\partial t}+\rho\frac{\partial(u_i k)}{\partial x_i}=\frac{\partial}{\partial x_j}\left[\left(\mu+\frac{\mu_t}{\sigma_k}\right)\frac{\partial k}{\partial x_j}\right]+G_k-Y_k+S_k+G_b \tag{4}$$

$$\rho\frac{\partial \omega}{\partial t}+\rho\frac{\partial(u_i \omega)}{\partial x_i}=\frac{\partial}{\partial x_j}\left[\left(\mu+\frac{\mu_t}{\sigma_\omega}\right)\frac{\partial \omega}{\partial x_j}\right]+G_\omega-Y_\omega+S_\omega+G_{\omega b} \tag{5}$$

where σ_k and σ_ω are the turbulent Prandtl numbers for k and ω, respectively. G_k represents the generation of turbulence kinetic energy due to mean velocity gradients. G_ω represents the generation of ω. Y_k and Y_ω represent the dissipation of k and ω due to turbulence. S_k and S_ω are user-defined source terms. G_b and $G_{\omega b}$ account for buoyancy terms.

2.3. Boundary conditions

To obtain simulation results that closely resemble real-world scenarios, we determine the fundamental boundary conditions for numerical simulations based on the experiment conducted by Yang et al. This experiment is carried out in a double-pipe heat exchanger, where the heating power is adjusted at a given flow rate to maintain a constant water temperature at the tube inlet. To minimize heat loss to the surroundings, the entire apparatus is effectively insulated.

The following boundary conditions and fluid properties are given in this work:

Wall: $u_w = v_w = w_w = 0$, $T_w = 350$K.

Inlet: $u_{in} = v_{in} = 0$, w_{in} = constant, $T_{in} = 300$K.

Outlet: The fluid at the outlet of the tube is in full-developed state, and the outlet pressure is adjusted to 1 atm.

It is assumed that the thermophysical properties of the fluid are constant: ρ = 998.2 kg/m^3, λ = 0.6 W/(m·K), $\mu = 1.003\times10^{-3}$ kg/(m·s), c_p = 4182 J/(kg·K). The current study is concerned with Re of 3000 to 11000.

2.4. Data reduction

The average temperature and pressure in the pipeline cross-sections are defined as follows:

$$\overline{T} = \frac{\iint_A uTdA}{\iint_A udA} \tag{6}$$

$$\overline{p} = \frac{\iint_A pdA}{\iint_A dA} \tag{7}$$

The heat transfer rate and the logarithmic mean temperature difference are defined as follows:

$$q = \frac{\dot{m}c_p(T_{m,in} - T_{m.out})}{A_w} \tag{8}$$

$$\Delta T = \frac{(T_w - T_{m,in}) - (T_w - T_{m,out})}{\ln\left(\frac{T_w - T_{m,in}}{T_w - T_{m,out}}\right)} \tag{9}$$

where A_w is the total heat transfer area of the TOT, and $T_{m,in}$ and $T_{m,out}$ are the mean temperature of the inlet and outlet.

The coefficient of convective heat transfer is defined as:

$$h_{avg} = \frac{q}{\Delta T} \tag{10}$$

The hydraulic diameter is defined as:

$$D_h = \frac{4A}{C} \tag{11}$$

where A is the cross-section area of the TOT, and C is the circumference of the ellipse.

The Reynolds number and average Nusselt number are defined as follows:

$$Re = \frac{\rho\omega_{in}D_h}{\mu} \tag{12}$$

$$\overline{Nu} = \frac{h_{avg}D_h}{\lambda} \tag{13}$$

where ω_{in} is the inlet velocity, and λ is the thermal conductivity.

The angle between the velocity vector and the temperature gradient is defined as follows:

$$\theta = \arccos \frac{\overline{U} \cdot \nabla \overline{T}}{\left|\overline{U}\right| \cdot \left|\nabla \overline{T}\right|} \tag{14}$$

Dimensionless parameters are utilized, defined as:

$$\overline{U} = \frac{U}{u_m} \tag{15}$$

$$\nabla \overline{T} = \frac{\nabla T}{(T_w - T_m)/H} \tag{16}$$

where U, u_m, ∇T, T_m and H are the velocity vector, main flow velocity, temperature gradient, main flow temperature and the height of the channel, respectively.

The performance evaluation criterion of the integral thermal-hydraulic for pipeline is defined as:

$$PEC = \frac{\overline{Nu}/\overline{Nu}_0}{(\Delta P/\Delta P_0)^{1/3}} \tag{17}$$

where the subscript 0 represents the SOT with the same cross-section as the TOT.

3. Results and discussion

3.1. Validation of numerical results

This study employed the fluid dynamics software FLUENT to simulate the fluid flow characteristics inside the pipeline. The models are divided using structured mesh, and the orthogonal quality of the meshes are all above 0.5. As the fluid flow near the wall surface is greatly influenced by molecular viscous forces, the mesh near the tube wall is finely divided. Figure 2 shows the meshing details of the TOT.

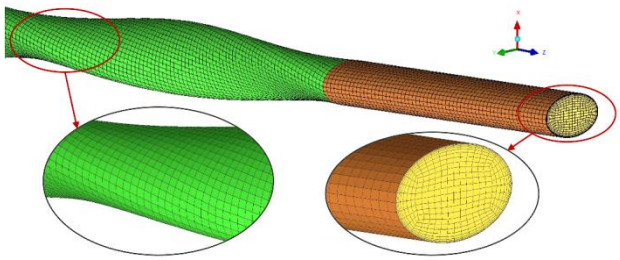

Figure 2. Meshing details of the TOT.

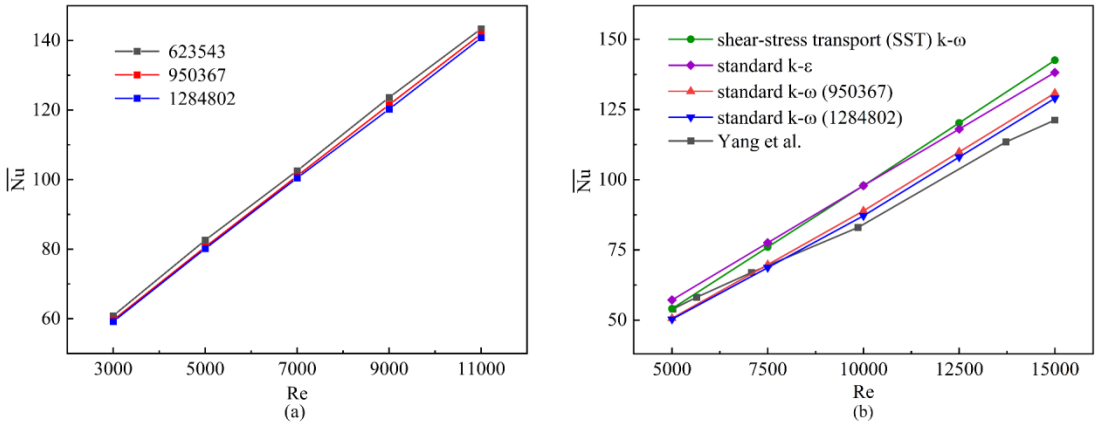

Figure 3. Mesh independence test and model variation.

In order to enhance the accuracy of numerical simulation results, mesh independence is verified by testing the $\overline{Nu}$ with a/b of 1.70 using different mesh numbers (623543, 950367, and 1284802). From Figure 3(a), The maximum error between the $\overline{Nu}$ with mesh numbers 950367 and 1284802 is below 1% in the range of Re between 3000 and 11000. Therefore, the TOT with mesh number 950367 is considered mesh independence. Figure 3(b) depicts the computational results of the *k-ε* model, the

standard *k-ω* model, the SST *k-ω* model and the experimental results tested by Yang et al [10]. The maximum error between the $\overline{Nu}$ calculated using the standard *k-ω* model and the data tested in the laboratory is 7.92% which the least error of all models. Therefore, this work also demonstrates the accuracy of the standard *k-ω* model in predicting the actual situation and utilizes it for the next numerical simulation studies.

3.2. Enhancement performance for TOT

This section studies the heat transfer and pressure drop characteristics of SCT, SOT and TOT. The a/b for the pipeline cross-section of the SOT and the TOT is 1.70.

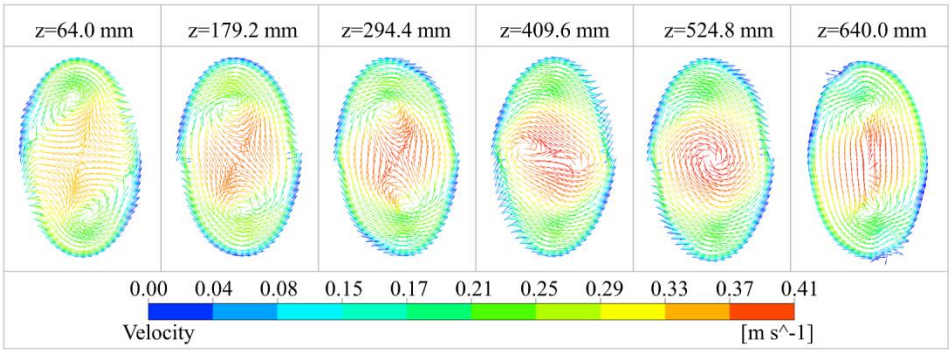

Figure 4. Velocity vector distributions in the TOT with a/b of 1.70.

The velocity vector distributions inside the TOT are shown in Figure 4. The fluid generates complex secondary flow due to the tangential stress of tube wall and turbulence disturbance as the fluid enters the twisted section from the upstream section. This leads to the rapid generation of two strong vortices at centrosymmetric locations on the major axis of the oval cross-section. As the flow develops further, the vortices gradually move closer the tube axis. Eventually, these vortices merge into a large vortex, which forms a helical flow inside the TOT. Therefore, the formation of helical flow in the TOT requires the fluid to undergo a series of development processes. The downstream tube wall destroys the stable helical flow when the fluid flows out of the twisted section and enters the downstream section. As a result, a difference in the velocity vector from the previous distribution can be clearly observed at the exit cross-section (z=640mm).

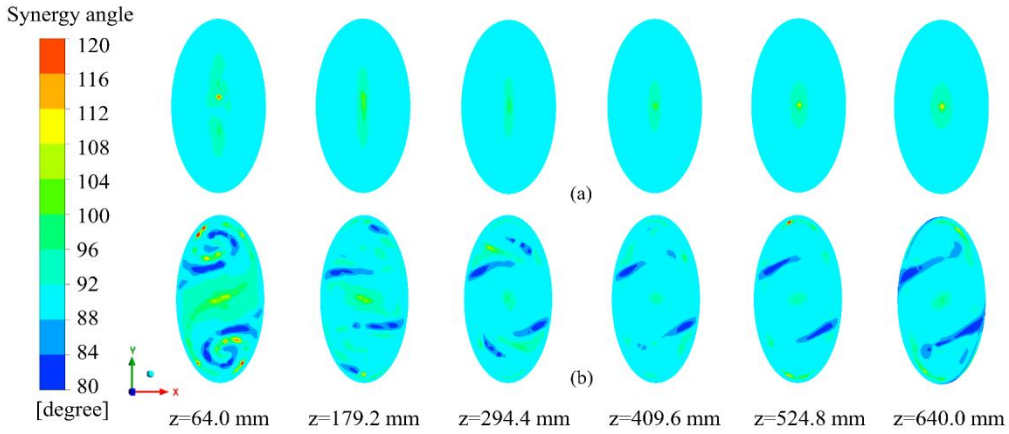

Figure 5. Local synergy angle distributions in the tube with a/b of 1.70. (a) SOT, (b) TOT.

The local synergy angle distributions inside the SOT and TOT with a/b of 1.70 is shown in Figure 5. The heat transfer capacity of the pipeline will be improved as the synergy angle approaches 0 degrees or 180 degrees. It is evident from Figure 5 that the synergy angle of the SOTs predominantly

ranges around 90 degrees except for the central area of the cross-section. However, significant regions with synergy angles greater than or less than 90 degrees are present in the TOTs. The presence of these regions greatly improves the heat transfer capacity of the TOT. The local synergy angle inside the tube appears significantly different compared to that of SOT when the fluid is just entering the twisted section from the upstream section. However, the improvement in the local synergy angle is diminished as a steady spiral flow forms in the tube. In addition, the steady helical flow developed inside the tube is again influenced by the structural changes of pipeline as the fluid enters the downstream section from the twisted section. As a result, the local synergy angle is again changed at the pipeline outlet cross-section (z=640 mm).

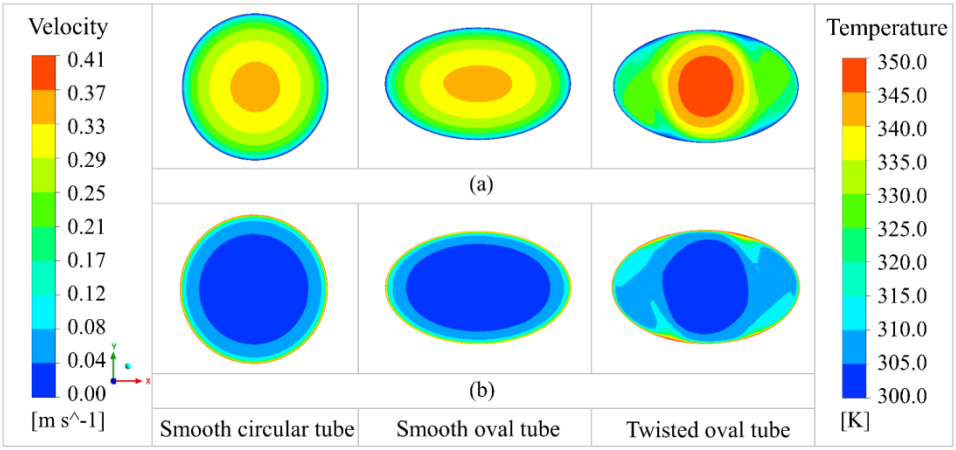

Figure 6. Velocity and temperature distribution in the cross-section of tubes with different shapes. (a) Velocity distribution, (b) Temperature distribution.

The velocity and temperature distribution of the different pipeline center sections (z=320mm) are shown in Figure 6. The Re of fluids at the tube inlet is 5000. The velocity and temperature contour of the SCT and SOT are concentric circular and concentric oval shapes, respectively. In the case of the TOT, after the fluid enters the tube, the twisted wall impedes the forward flow of the fluid, resulting in a scouring effect on the tube wall. This phenomenon leads to a thinning of the fluid boundary layer at corresponding positions and an increase in temperature gradient, thereby enhancing the heat transfer between the tube wall and the fluid. This also leads to significant changes of temperature distribution inside the tube. From Figure 6, the temperature distribution contour of the TOT is twisted at both ends of the major axis. In addition, there is a significant high-speed flow area in the pipeline center due to the blockage and shear stress of twisted wall.

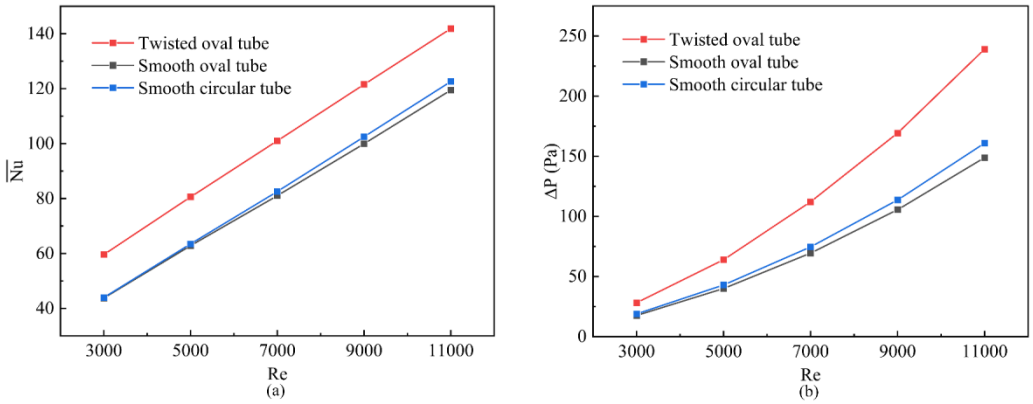

Figure 7. Averaged Nusselt number and pressure drop in tubes of different shapes.

The $\overline{Nu}$ and pressure drop in different tubes are shown in Figure 7. The trend of $\overline{Nu}$ variation is consistent among the three types of tubes within the range of Re from 3000-11000. Moreover, the $\overline{Nu}$ for each tube has a linear relationship with the Re. Due to the increase in the cold fluid quality in the pipeline with increasing Re, which causes an increased the heat transfer efficiency of tube wall. Additionally, the increase in fluid velocity increases the turbulence intensity, which further promotes heat transfer. Therefore, the $\overline{Nu}$ increases as the Re increases. The $\overline{Nu}$ for TOT increased by 18.7%-35.5% compared to SOTs at the same Re. This means that TOT have better heat transfer properties. However, the pressure drop of the TOT also increases by 59.9%-61.3% simultaneously, indicating that TOT requires more energy to maintain fluid flow inside the tube compared to SOT. The SOT and SCT have the same hydraulic diameter, so there is not much difference in the $\overline{Nu}$ and pressure drop between the two. However, the difference between the two also increases gradually as the increasing Re.

The $\overline{Nu}$ and pressure drop of TOT comparison with that of SOT is shown in Figure 8. The $\overline{Nu}/\overline{Nu_0}$ decreases from 1.36 to 1.19 when the Re increases from 3000 to 11000. This indicates that the enhanced heat transfer effect of the TOT decreases with increasing Re. However, the TOT always has better heat transfer effect than the SOT. The pressure drop ratio of the TOT and SOT with the same tube cross-section is almost independent of the Re. From Figure 8, the $\Delta P/\Delta P_0$ is about 1.6 with a/b of 1.70.

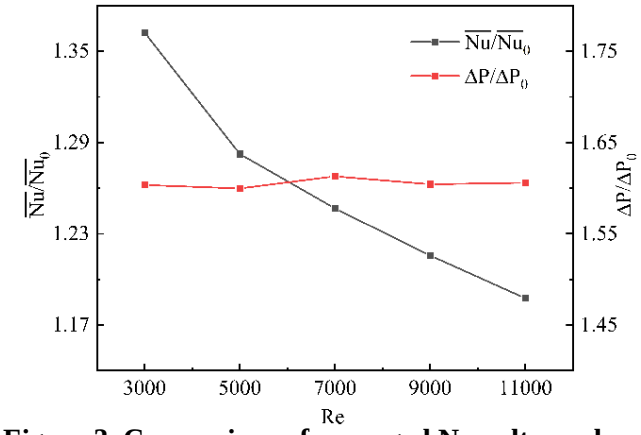

Figure 3. Comparison of averaged Nusselt number and pressure drop for the TOT and the SOT.

3.3. Effect of a/b on enhanced performance

This section investigates the effect of a/b and Re on the heat transfer and pressure drop characteristics of TOTs and evaluates integral thermal-hydraulic effectiveness of the pipeline.

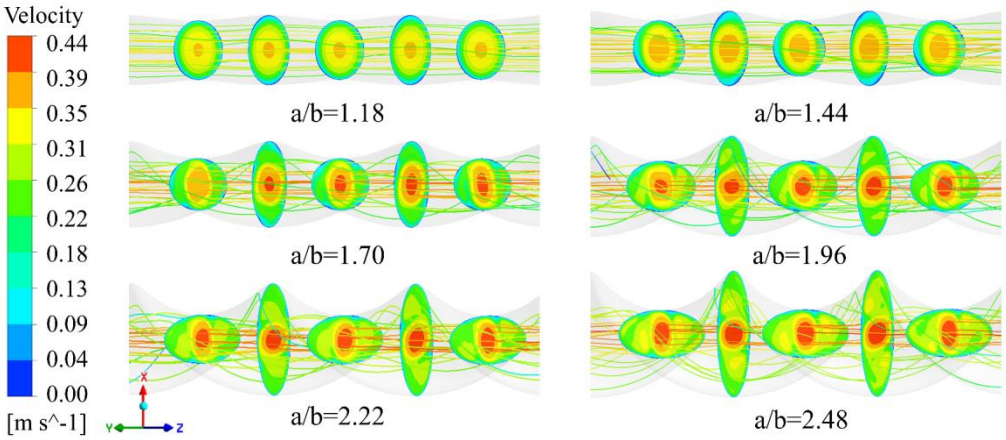

Figure 9. Streamline and velocity distribution in TOTs with different a/b.

The streamlines and velocity distribution inside TOTs with different a/b are shown in Figure 9. The tube cross-sections are shown from z=256mm to z=384mm with the inlet fluid Re of 5000. The streamlines near the tube axis are distributed axially. However, the fluid near the TOT wall is blocked by the twisted wall, so that the streamlines are spirally distributed. The spiral flow in tube creates

secondary flows, which breaks the fluid boundary layer. Therefore, the thickness of the boundary layer decreases as increasing a/b. In the TOT with a/b of 1.18, spiral streamlines are not obvious because a/b is too small. In addition, the fluid velocity in the twisted tube center increases as a/b increases.

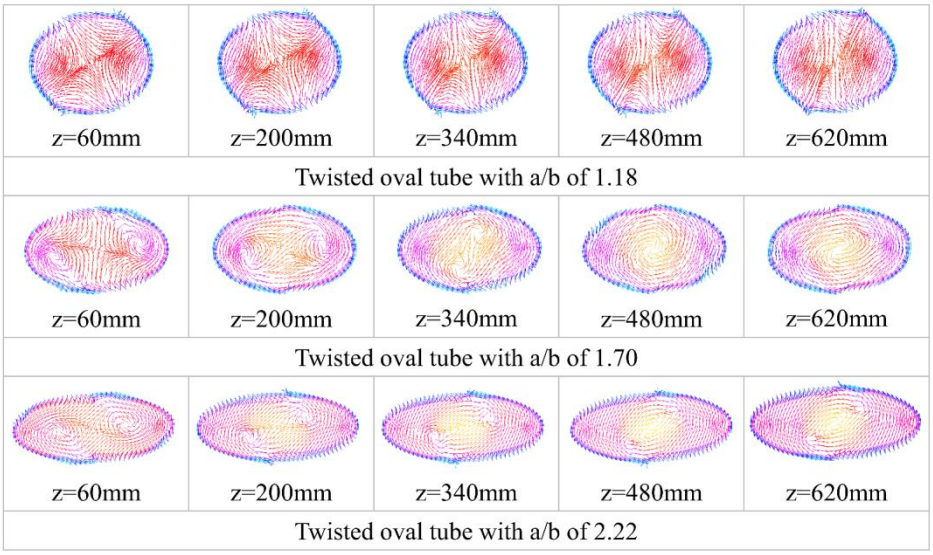

Figure 10. Velocity vector distributions in the cross-section of the TOTs.

The fluid velocity vector distributions inside the TOT with a/b of 1.18, 1.70 and 2.22 are shown in Figure 10. In the TOT with the a/b of 1.18, there are no regular vortices inside the tube as the wall has less influence on the flow. However, the fluid clearly generates a certain intensity of secondary flow in the TOT, which contributes to enhanced heat transfer of pipeline. In the TOTs with a/b of 1.70 and 2.22, the rapid generation of two strong vortices at centrosymmetric locations on the major axis of the oval cross-section when the fluid enters the twisted section from the upstream section. As the flow develops further, the vortices eventually merge into a large vortex, which forms a spiral flow. By comparing the velocity vector distribution at a/b of 1.70 and 2.22, the larger the a/b, the longer the flow process required for the eddies to converge to form the spiral flow. This is because the intensity of spiral flow varies with different a/b, resulting in differences in the formation process of spiral flow. Combined with the streamline diagram, it can be deduced that the two stronger vortices are distributed in a double helix in the TOT before converging.

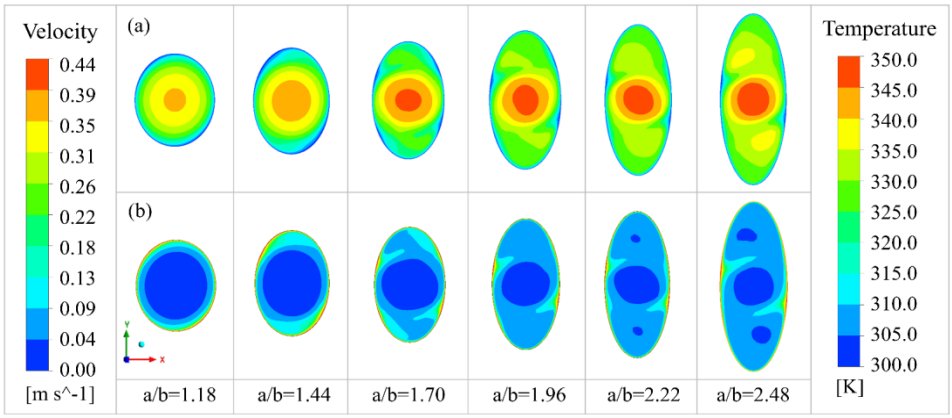

Figure 11. Velocity and temperature distributions in the cross-section of the TOTs with different a/b. (a) Velocity distributions, (b) Temperature distributions.

The velocity and temperature distribution of the pipeline center cross-section (z=320 mm) of the TOT are shown in Figure 11. The low-temperature fluid near the tube wall increases with the increase of a/b. In the TOTs with a/b of 2.22 and 2.48, two more mainstream regions appear in addition to the central region of the tube cross-section. Combined with the velocity vector distribution of the fluid in the pipeline, it can be concluded that the two main flow regions on the elliptic section are caused by the vortex in the tube.

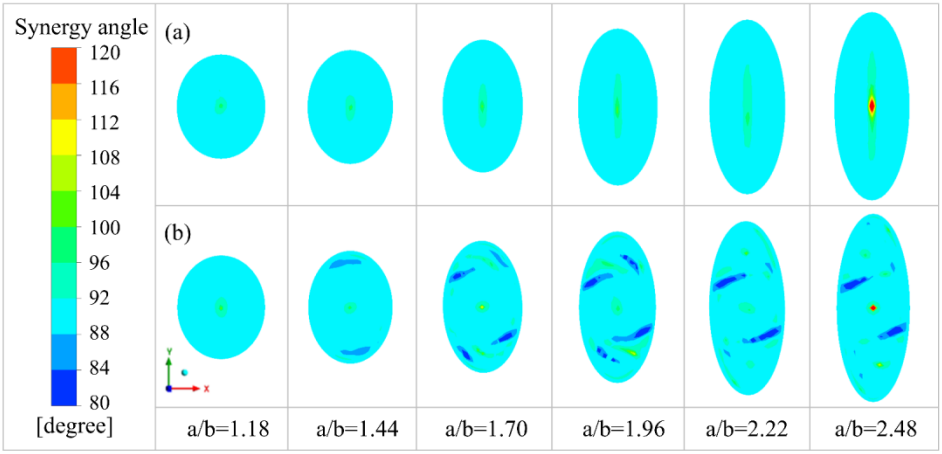

Figure 12. Local synergy angle distributions in the cross-section of tubes with different a/b. (a)SOTs, (b) TOTs.

The local synergy angle distributions of the pipeline center cross-section (z=320 mm) of SOTs and TOTs with different a/b are shown in Figure 12. The synergy angle of the SOTs predominantly ranges around 90 degrees except for the central area of the cross-section. However, significant regions with synergy angles less than 90 degrees are present in the TOTs. According to the synergy angle distributions of the TOTs, the degree of improvement in the synergy angle does not always increase with increasing a/b. Numerical simulation results show that the largest synergy angle of 113 degrees occurred in the cross-section with a/b of 1.70 and the smallest synergy angle of 67 degrees occurred in the cross-section with a/b of 1.96. The synergy angle distribution inside different pipelines are complex because of the different processes by which the fluid forms a spiral flow in different TOTs. Therefore, it is not possible to determine the TOT with the best enhanced heat transfer simply on the basis of the synergy angle distribution at z=320 mm.

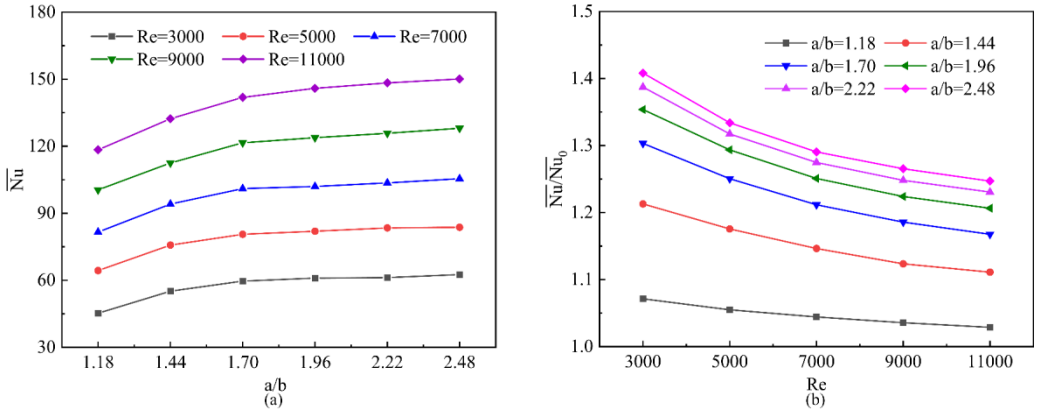

Figure 13. Averaged Nusselt number in the TOTs and comparison of averaged Nusselt number for the TOTs and the SOTs.

Figure 13 shows the $\overline{Nu}$ in the TOTs with different a/b, as well as its comparison with that in the SOTs. Owing to the blocking influence of the twisted wall, which makes the fluid disturbance more intense, thereby enhancing the heat transfer efficiency of the pipeline. Therefore, the $\overline{Nu}$ increases as the increasing Re and increasing a/b. However, the magnitude of the increase in the $\overline{Nu}$ gradually decreases as the a/b increases. More specifically, in the case of a/b less than 1.96, the increase of $\overline{Nu}$ by increasing a/b is more obvious, which indicates that the structural dimensions of the TOT are the major influencing elements in this case. In the case of a/b greater than 1.96, the effect of increasing a/b on the $\overline{Nu}$ is weaker, but the difference of the $\overline{Nu}$ at different Re is obvious, which indicates that the Re becomes the main influencing factor in this case. The simulation results show that the $\overline{Nu}$ of the TOTs increases by 26.7%-38.2% as a/b increases from 1.18 to 2.48.

The $\overline{Nu}/\overline{Nu_0}$ decreases with increasing Re. This indicates that the impact of the twisted wall on enhanced heat transfer diminishes as the Re increases. However, the heat transfer of the TOT is still enhanced compared to the SOT. Moreover, among the six different models of TOTs, the one with a/b of 1.18 exhibits the weakest effect on enhancing heat transfer. Therefore, the ratio of its $\overline{Nu}$ to that of the smooth tube is closest to 1.0.

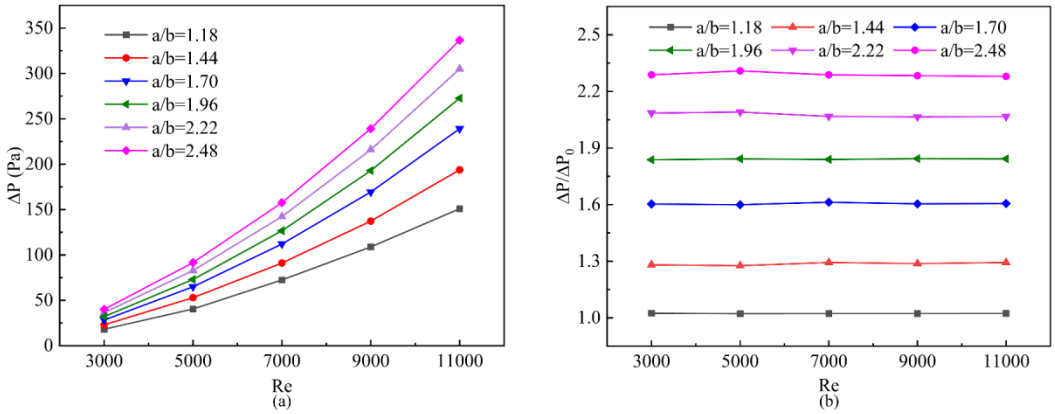

Figure 14. Pressure drop in the TOTs and comparison of pressure drop for the TOTs and SOTs.

The increase in flow velocity results in a variation in pressure drop. Figure 14 depicts the change of pressure drop in the TOTs with different a/b at different Re and its comparison with that in the SOTs. The pressure drop increases with increasing Re and increasing a/b. And the $\Delta P/\Delta P_0$ is almost unaffected by the Re. For Re from 3000 to 11000, the pressure drop inside the TOTs with a/b of 1.18, 1.44, 1.70, 1.96, 2.22 and 2.48 are about 1.02, 1.28, 1.60, 1.84, 2.07 and 2.28 times of that inside the SOTs with the same tube cross-section, respectively. In this regard, it is evident that the increase of a/b significantly enhances the pressure drop inside the TOT.

The integral thermal-hydraulic effectiveness of TOTs is shown in Figure 15. In the case of the Re of inlet fluid is determined, the turbulence intensity of the fluid inside the pipeline increases as an increasing a/b, which strengthen the heat transfer efficiency of TOTs. The integral thermal-hydraulic effectiveness of the tube is enhanced when the impact of the TOT to enhance heat transfer is larger than the increment of flow resistance. However, when a/b exceeds a certain threshold, the flow

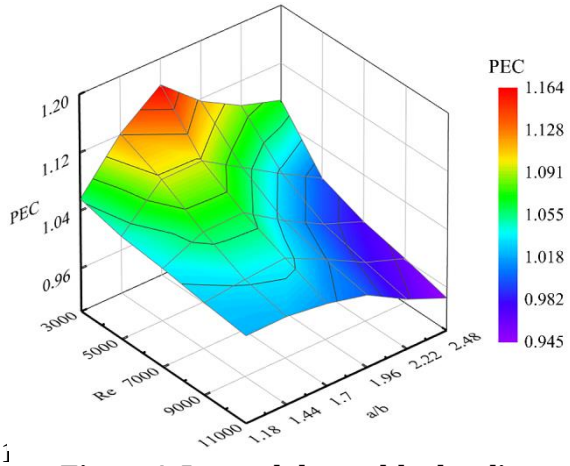

Figure 4. Integral thermal-hydraulic effectiveness of TOTs.

resistance increment dominates and leads to a decrease in the integral thermal-hydraulic effectiveness. Numerical simulations indicate that the integral thermal-hydraulic effectiveness of TOTs with a/b in the range of 1.40 to 1.96 is superior to other pipeline models under Re ranging from 3000 to 11000. Additionally, TOTs exhibit better enhanced heat transfer characteristics at lower Re based on the results of the study.

4. Conclusions

The study aims to investigate the performance difference of SCT, SOT and TOT at the same hydraulic diameter using numerical simulations. The impact of the a/b on the fluid flow inside the TOT is investigated. The integral thermal-hydraulic effectiveness of TOT is assessed and the summary of the flow law within the TOTs is presented. The main results are as follows:

(1) Due to the twisted wall, the TOT enhances the heat transfer between the tube wall and the fluid, but also increases the flow resistance. The $\overline{Nu}$ of TOT with a/b of 1.70 increases by 18.7%-35.5% and the pressure drop increases by 59.9%-61.3% compared with SOT.

(2) In the TOT with a/b of 1.70, two pronounced vortices are rapidly generated inside the TOT as the fluid enters the twisted section from the upstream section. As the fluid develops further, the vortices converge and eventually form a spiral flow. The two stronger vortices are distributed in a double helix inside the TOT before convergence.

(3) In the case of the Re of inlet fluid is determined, the turbulence intensity inside the TOT increases with increasing a/b. However, when a/b exceeds a certain threshold, the increased flow resistance leads to a decrease in integral thermal-hydraulic effectiveness. Numerical simulations show that TOTs with a/b ranging from 1.40 to 1.96 exhibit superior performance compared to other tubes.

Nomenclature

A –cross-section area of the tubes, [mm^2]
A_w –area of heat transfer tube wall, [mm^2]
a –major axis of the oval cross-section, [mm]
b –minor axis of the oval cross-section, [mm]
C –circumference of the ellipse, [mm]
C_p –specific heat capacity, [$Jkg^{-1}K^{-1}$]
D_h –hydraulic diameter of the tubes, [mm]
H –height of the channel, [mm]
h_{avg} –heat transfer coefficient, [$Wm^{-2}K^{-1}$]
k –turbulence kinetic energy, [m^2s^{-2}]
L –length of the twisted oval tubes, [mm]
L_{in} –twisted oval tubes upstream length, [mm]
L_{out} –twisted oval tubes downstream length, [mm]
$\dot{m}$ –mass flow rate, [$kg{\cdot}s^{-1}$]
Nu –Nusselt number, [–]
$\overline{Nu}$ –averaged Nusselt number, [–]
p –pressure, [Pa]
Δp –pressure drop, [Pa]
q –heat transfer rate, [Wm^{-2}]
Re –Reynolds number, [–]
S –360° twist spacing of twisted oval tubes, [mm]
ΔT –temperature difference, [K]
u, v, w –velocity components, [$m{\cdot}s^{-1}$]
U –fluid velocity vector, [$m{\cdot}s^{-1}$]
x, y, z –x, y and axial direction coordinates, [–]

Greek letters

ρ –density, [kgm^{-3}]
μ –dynamic viscosity, [Pa·s]
λ –thermal conductivity, [$Wm^{-1}K^{-1}$]
θ –angle between the velocity vector and the temperature gradient, [degree]
ω –specific dissipation rate, [s^{-1}]
ε –turbulence kinetic energy, [m^2s^{-2}]

Subscripts

f –fluid
in –inlet
int –internal
m –main flow
out –outlet
t –turbulent

t	–time, [s]	w	–wall
T	–temperature, [K]	0	–smooth oval tubes

References

[1] Liu, Y., *et al.*, Process modelling, optimisation and analysis of heat recovery energy system for petrochemical industry, *Journal of Cleaner Production*, *381*. (2022), DOI No. 10.1016/j.jclepro.2022.135133

[2] Sadeghianjahromi, A.,C.-C. Wang, Heat transfer enhancement in fin-and-tube heat exchangers – A review on different mechanisms, *Renewable and Sustainable Energy Reviews*, *137*. (2021), DOI No. 10.1016/j.rser.2020.110470

[3] Hosseini, A.M.,A. Faghih Khorasani, Experimental and numerical study of the rib effect in a gas-gas heat exchanger performance used in a sponge iron production plant (MIDREX), *Proceedings of the Institution of Mechanical Engineers, Part A: Journal of Power and Energy*, *235*. (2021), 7, pp. 1747-1758, DOI No. 10.1177/09576509211007969

[4] Walraven, D., *et al.*, Comparison of shell-and-tube with plate heat exchangers for the use in low-temperature organic Rankine cycles, *Energy Conversion and Management*, *87*. (2014), pp. 227-237, DOI No. 10.1016/j.enconman.2014.07.019

[5] Manjunath, K.,S.C. Kaushik, Second law thermodynamic study of heat exchangers: A review, *Renewable and Sustainable Energy Reviews*, *40*. (2014), pp. 348-374, DOI No. 10.1016/j.rser.2014.07.186

[6] Hajmohammadi, M.R., *et al.*, Heat transfer improvement due to the imposition of non-uniform wall heating for in-tube laminar forced convection, *Applied Thermal Engineering*, *61*. (2013), 2, pp. 268-277, DOI No. 10.1016/j.applthermaleng.2013.08.009

[7] Zhang, L., *et al.*, Experimental study on condensation heat transfer characteristics of steam on horizontal twisted elliptical tubes, *Applied Energy*, *97*. (2012), pp. 881-887, DOI No. 10.1016/j.apenergy.2011.11.085

[8] Li, X., *et al.*, Research progress and application of heat transfer enhancement of twisted oval tubes, *The Chinese Journal of Process Engineering*, *22*. (2022), 5, pp. 561-572

[9] Man, C., *et al.*, The experimental study on the heat transfer and friction factor characteristics in tube with a new kind of twisted tape insert, *International Communications in Heat and Mass Transfer*, *75*. (2016), pp. 124-129, DOI No. 10.1016/j.icheatmasstransfer.2016.04.003

[10] Yang, S., *et al.*, Experimental study on convective heat transfer and flow resistance characteristics of water flow in twisted elliptical tubes, *Applied Thermal Engineering*, *31*. (2011), 14-15, pp. 2981-2991, DOI No. 10.1016/j.applthermaleng.2011.05.030

[11] Tan, X.-h., *et al.*, Experimental and numerical study of convective heat transfer and fluid flow in twisted oval tubes, *International Journal of Heat and Mass Transfer*, *55*. (2012), 17-18, pp. 4701-4710, DOI No. 10.1016/j.ijheatmasstransfer.2012.04.030

[12] Cheng, J., *et al.*, Analysis of heat transfer and flow resistance of twisted oval tube in low Reynolds number flow, *International Journal of Heat and Mass Transfer, 109*. (2017), pp. 761-777, DOI No. 10.1016/j.ijheatmasstransfer.2017.02.061

[13] Guo, A.-N.,L.-B. Wang, Parametrization of secondary flow intensity for laminar forced convection in twisted elliptical tube and derivation of loss coefficient and Nusselt number correlations by numerical analysis, *International Journal of Thermal Sciences, 155*. (2020), DOI No. 10.1016/j.ijthermalsci.2020.106425

[14] Guo, A.-N.,L.-B. Wang, The mechanism of laminar convective heat transfer enhancement enforced by twisting of elliptical tube, *International Journal of Heat and Mass Transfer, 157*. (2020), DOI No. 10.1016/j.ijheatmasstransfer.2020.119961

[15] Wu, C.-C., *et al.*, Numerical simulation of turbulent flow forced convection in a twisted elliptical tube, *International Journal of Thermal Sciences, 132*. (2018), pp. 199-208, DOI No. 10.1016/j.ijthermalsci.2018.05.028

[16] Gu, H., *et al.*, Performance investigation on twisted elliptical tube heat exchangers with coupling-vortex square tube layout, *International Journal of Heat and Mass Transfer, 151*. (2020), DOI No. 10.1016/j.ijheatmasstransfer.2020.119473

[17] Gu, H., *et al.*, Influence of alternating V-rows tube layout on thermal-hydraulic characteristics of twisted elliptical tube heat exchangers, *International Journal of Heat and Mass Transfer, 159*. (2020), DOI No. 10.1016/j.ijheatmasstransfer.2020.120070

[18] Li, X., *et al.*, Study on shell side heat transport enhancement of double tube heat exchangers by twisted oval tubes, *International Communications in Heat and Mass Transfer, 124*. (2021), DOI No. 10.1016/j.icheatmasstransfer.2021.105273

[19] Li, X., *et al.*, Experimental study on heat transfer and pressure drop of twisted oval tube bundle in cross flow, *Experimental Thermal and Fluid Science, 99*. (2018), pp. 251-258, DOI No. 10.1016/j.expthermflusci.2018.07.030

[20] Gu, X., *et al.*, Heat Transfer and Flow Resistance Characteristics of Helical Baffle Heat Exchangers with Twisted Oval Tube, *Journal of Thermal Science, 31*. (2022), 2, pp. 370-378, DOI No. 10.1007/s11630-022-1581-1

[21] Luo, C.,K. Song, Thermal performance enhancement of a double-tube heat exchanger with novel twisted annulus formed by counter-twisted oval tubes, *International Journal of Thermal Sciences, 164*. (2021), DOI No. 10.1016/j.ijthermalsci.2021.106892

[22] Jing, D., *et al.*, Size dependences of hydraulic resistance and heat transfer of fluid flow in elliptical microchannel heat sinks with boundary slip, *International Journal of Heat and Mass Transfer, 119*. (2018), pp. 647-653, DOI No. 10.1016/j.ijheatmasstransfer.2017.11.149

Received: 14.07.2023.
Revised: 31.10.2023.
Accepted: 14.11.2023.